Chinese Chemical Letters 37 (2026) 111914

Contents lists available at ScienceDirect

Chinese Chemical Letters

journal homepage: www.elsevier.com/locate/cclet

Efficient copper sorption from saline wastewater using citrate-modified biochar with robust anti-salt interferences

Xianxin Luo[a,b], Jianhao Xu[b], Qi Luo[b], Yan Xiao[b], Feng Wei[c], Meitong Li[d], Wenjiao Yuan[d], Penghui Shao[b,*], Shenglian Luo[a,b,*]

[a] College of Environmental Science and Engineering, Hunan University, Changsha 410082, China
[b] College of Environmental and Chemical Engineering, Nanchang Hangkong University, Nanchang 330063, China
[c] Jiangxi Hongcheng Environment Co., Ltd., Nanchang 330038, China
[d] School of Environmental Science and Safety Engineering, Tianjin University of Technology, Tianjin 300384, China

ARTICLE INFO

Article history:
Received 1 April 2025
Revised 12 August 2025
Accepted 28 September 2025
Available online 28 September 2025

Keywords:
Biochar
Copper
Adsorption
Citrate modification
High-salinity wastewater

ABSTRACT

Eliminating heavy metals from industrial high-salinity wastewater is imperative for sustainable industrial development and environmental protection. Herein, a citrate-modified biochar that demonstrated robust anti-salt interference was developed. The sorbent achieved an adsorption capacity of 252.14 mg/g in 4.1 mol/L NaCl solution and 232.55 mg/g in 1.4 mol/L Na_2SO_4 solution, maintaining efficient Cu(II) adsorption over four cycles. It retained an adsorption capacity of 236.89 mg/g in real waste salt-derived brine. Adsorption followed *pseudo*-first-order kinetics ($k = 0.0901\ min^{-1}$) and conformed to the Langmuir isotherm ($q_{max} = 251.21$ mg/g) model, indicating that physical adsorption on a homogeneous surface primarily governs the adsorption mechanisms. Thermodynamic analysis revealed that the adsorption is spontaneous and endothermic, with enhanced affinity for Cu(II) at higher temperatures. Oxygen-containing groups, especially the hydroxyl group, drove adsorption *via* surface precipitation/complexation, ultimately generating posnjakite ($Cu_4(SO_4)(OH)_6{\cdot}2H_2O$). Cost analysis showed that the total expenditure for treating 1000 L of wastewater (300 mg_{Cu}/L) was \$28.89 (\$0.0963/$g_{Cu(II)}$) and the treatment capacity using fixed-bed columns was 120 L/kg. These findings offer a viable and cost-effective strategy for Cu(II) elimination from high-salinity wastewater.

© 2026 Published by Elsevier B.V. on behalf of Chinese Chemical Society and Institute of Materia Medica, Chinese Academy of Medical Sciences.

Heavy metals (HMs) are extensively applied across numerous industrial enterprises, including traditional sectors like textile manufacturing, tannery, and printing/dyeing [1,2], as well as emerging energy industries typified by lithium-ion battery (LIB) production, where copper accounts for 7.3 %–16.6 % of battery mass as the current collector in anode materials [3–5]. Improper discharge of copper-laden wastewater threatens aquatic ecosystems and human health due to their inherent toxicity and non-biodegradable properties [6]. This concern has prompted the U.S. EPA to establish a strict 1.3 mg/L effluent limit for copper [1].

High-salinity industrial wastewater and waste salts often contain HMs [6–9]. Current recycling techniques for high-salinity wastewater primarily rely on advanced membrane methods, such as nanofiltration, electroosmosis, and capacitive deionization [10]. However, the presence of HMs in these solutions can cause severe membrane fouling, which increases energy consumption and reduces recycling efficiency [11]. Therefore, there is an urgent need to develop efficient and scalable technologies for removing HMs from both industrial wastewater and waste salt brine, enabling sustainable resource recycling and utilization.

Adsorption is preferred over other heavy metal remediation techniques, particularly for biochar-based sorbents, which stand out for their renewable feedstocks, facile fabrication, and cost-effectiveness [12–15]. For instance, Elgarahy *et al.* [12] developed a multifunctional eco-friendly sorbent derived from marine brown algae and bivalve shells, achieving a Cu(II) adsorption capacity of 6.94 mmol/g. Radenković *et al.* [13] utilized a renewable and locally available sunflower waste to fabricate a highly microporous adsorbent for copper removal from heavily polluted mining drainage water, emphasizing its alignment with the principles of green chemistry and circular economy. Zhao *et al.* [14] synthesized pomelo peel biochar *via* a facile low-temperature one-step approach, yielding 137.4 mg/g Ag(I) and 88.7 mg/g Pb(II) adsorption capacities. Biswal and Balasubramanian [15] conducted a comparative analysis of heavy metal removal techniques, concluding that adsorption-based remediation is both efficient and cost-effective

* Corresponding authors.
E-mail addresses: penghui_shao@163.com (P. Shao), sllou@hnu.edu.cn (S. Luo).

https://doi.org/10.1016/j.cclet.2025.111914
1001-8417/© 2026 Published by Elsevier B.V. on behalf of Chinese Chemical Society and Institute of Materia Medica, Chinese Academy of Medical Sciences.

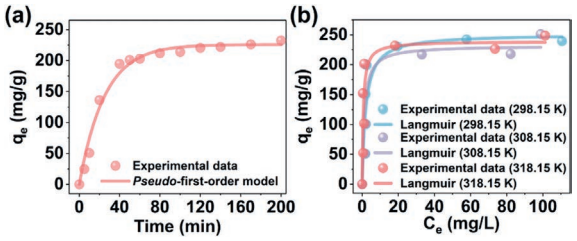


Fig. 1. The optimal fitting pattern for (a) the *pseudo*-first-order kinetic model and (b) Langmuir isotherm model in describing Cu(II) adsorption using CBC sorbent. The initial Cu(II) concentration in kinetic assay was 250 mg/L, whereas for the isotherm assays, a series of initial concentrations, including 0, 50, 100, 150, 200, 250, 300, 350 mg/L were employed.

for practical applications. Additionally, the citrate-modified rice straw biochar was developed to address the issues of silicon deficiency and HMs pollution in farmland soil, achieving Cu(II) adsorption capacity of 271.73 mg/g [16].

However, high salinity may significantly influence sorbent's performance in adsorbing HMs. Wang *et al.* [17] proposed that elevated salinity can reduce Cu(II) adsorption capacity because Na^+ competes for cation-exchange sites, weakening the electrostatic interactions with target HMs. Conversely, Chen *et al.* [18] demonstrated that Cl^- binding on sorbent surfaces enhanced Cu^{2+} attraction by counteracting electrostatic repulsion. Li *et al.* [19] incorporated zeolitic imidazolate framework-8 into membranes, achieving a nickel adsorption capacity of 219.09 mg/g in synthetic high-salinity ($[Na^+] = 15{,}000$ mg/L) wastewater. Chen *et al.* [20] reported a Cu(II) adsorption capacity of 81.91 mg/g using magnetic biochar derived from pomelo peel, which remained relatively stable in up to 1.0 mol/L Na^+ solution. Bogusz *et al.* [21] demonstrated 87 % Cu(II) removal in a 2.0 mol/L Cl^- solution using pyrolyzed biochar derived from *S. hermaphrodita* biomass. Babeker *et al.* [22] fabricated a chelating agent-modified biochar to enable effective Cu(II) adsorption, achieving a capacity of 196.68 mg/g in 500 mmol/L Na^+ solution. Despite these advancements, enhancing sorbents' anti-salt capacity and validating their performance in real brines remains a critical research priority.

This work preliminarily fabricated a biochar composite *via* a straightforward and eco-friendly pyrolysis method (Fig. S1a in Supporting information) to address Cu(II) removal in high-salinity wastewater. Physicochemical properties of the biochar were characterized and its adsorption performance under different conditions was analyzed, particularly in terms of anti-salt interference and effectiveness in real waste salt brine. Investigations into the underlying mechanisms of Cu(II) adsorption focused on the potential functional groups, crystalline phases, and surface chemical compositions of both pristine CBC and Cu(II)-adsorbed CBC in salt-free and salt-saturated conditions.

After evaluating five common biomass precursors, camphor bark was selected to fabricate a biochar sorbent *via* eco-friendly pyrolysis. The raw biochar achieved an adsorption capacity of 76.59 mg/g for Cu(II) (Fig. S1b in Supporting information). Among various modification strategies, citrate modification significantly enhanced adsorption capacity to 220.50 mg/g (Fig. S1c in Supporting information), representing a 2.88-fold improvement compared to raw biochar. The adsorption kinetics of Cu(II) onto citrate-modified biochar (CBC) sorbent were investigated at initial concentrations of 50 mg/L and 250 mg/L to assess the adsorption rate. The *pseudo*-first-order (PFO), *pseudo*-second-order (PSO), Elovich, and intra-particle diffusion models were employed to fit the experimental data. As shown in Fig. 1a and Table S2 (Supporting information), the PFO model provided the best fit ($R^2 = 0.9869$ and 0.9835) and the theoretical capacities ($q_t = 50.29$ mg/g and 225.81 mg/g) closely matched the experimental data (q_{max} of 50 mg/g and 232.54 mg/g). Equilibrium was reached after 30 min for the 50 mg/L solution (Fig. S5a in Supporting information) and 40 min for the 250 mg/L solution (Fig. 1a). This observation indicates that rapid surface physisorption dominates the adsorption process, with rates governed by adsorbate diffusion kinetics [23], and supports the hypothesis that Cu(II) uptake occurs primarily *via* outer-surface physisorption [24]. Meanwhile, the kinetic constant for the lower Cu(II) concentration (50 mg/L, $k_1 = 0.0901$) was 2.26 times higher than that of the higher concentration (250 mg/L, $k_1 = 0.0399$), implying enhanced physical adsorption efficiency under lower concentration conditions. Nevertheless, comparable R^2 values for both PFO and PSO models also imply potential synergistic contributions from both physisorption and chemisorption mechanisms, corroborating findings reported by Vikrant *et al.* [25]. Figs. S5b and c (Supporting information) depict the profiles of the intraparticle diffusion model at initial Cu(II) concentrations of 50 and 250 mg/L. Intra-particle diffusion analysis revealed three kinetic phases with a better fit for experimental data, including rapid surface complexation ($k_1 = 9.85$–50.95 mg g^{-1} $min^{-1/2}$), rate-limiting pore diffusion ($k_2 = 6.07$–26.15 mg g^{-1} $min^{-1/2}$), and equilibrium ($k_3 = 1.45$–13.08 mg g^{-1} $min^{-1/2}$) (Table S2 in Supporting information). The higher k_1 values indicates rapid Cu(II) adsorption *via* surface functional group complexation at external surface, while the reduced k_2 at higher concentrations implies saturation of active sites, likely governed by membrane and intra-particle diffusion [26]. Collectively, these results indicate that Cu(II) adsorption on the CBC sorbent involves multifaceted mechanisms, predominantly driven by physical processes. The superiority of the PFO model suggests that adsorbate diffusion dynamics govern the rate-limiting step, while the comparable PSO model also implies a potential contribution of chemisorption.

Adsorption isotherms of Cu(II) on CBC sorbent were evaluated at 298.15, 308.15, and 318.15 K. The evaluation utilized several models, including Langmuir, Freundlich, Temkin, Redlich-Peterson, and D-R. As shown in Fig. 1b and Fig. S6 (Supporting information), and Table S3 (Supporting information), the Langmuir isotherm model provided a better fit than Freundlich model, based on the correlation coefficients (R^2). The calculated q_L values (251.21 mg/g at 298.15 K, 231.86 mg/g at 308.15 K, and 239.03 mg/g at 318.15 K) closely matched experimental q_{max} values (239.43, 251.23, and 248.72 mg/g), indicating that monolayer adsorption occurred on homogeneous surfaces with equivalent adsorption sites [27]. The Langmuir constant (K_L) increased with temperature, reflecting enhanced Cu(II) affinity [28]. The calculated R_L values (0.0018–0.0390) confirmed favorable adsorption (Fig. S7 in Supporting information) [29–31]. The decreasing R_L with increasing temperature and initial concentration further indicated temperature-dependent endothermic behavior [18,27]. Freundlich model showed $n < 1.0$ and higher K_F values, indicating that Cu(II) adsorption is favorable on heterogeneous biochar surfaces [32]. Temkin isotherm model revealed a sorption energy (b_{Tem} ~100 J/mol) consistent with physical interactions (<8 kJ/mol). The lower sorption energy results from weak van der Waals forces and weak sorbent-sorbate interactions, suggesting that Cu(II) adsorption on the CBC is characterized by physical adsorption mechanisms, such as electrostatic attraction on the surface or interface [33,34]. D-R model-derived mean free energy ($E = 0.8588$–2.2445 kJ/mol) further supported physical interactions that predominantly governed the adsorption [34]. Redlich-Peterson model with β values approaching 1.0 validated monolayer adsorption on homogeneous sites [34]. Collectively, these results indicate that Cu(II) adsorption on CBC sorbent is primarily governed by physical mechanisms, including electrostatic interactions and surface complexation, with monolayer coverage favored at elevated temperatures.

The thermodynamic parameters, including standard enthalpy change (ΔH^0), free energy change (ΔG^0), and entropy change

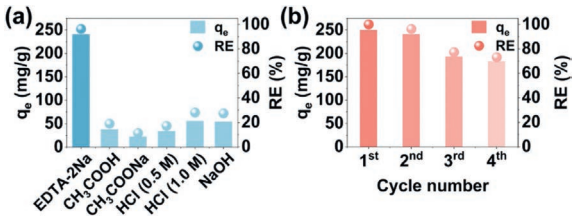


Fig. 2. The (a) screening of eluents for Cu(II) desorption from spent CBC sorbent and (b) recycling performance of CBC sorbent in Cu(II) adsorption after elution by EDTA-2Na. M = mol/L.

(ΔS^0), were analyzed to elucidate the energetics and spontaneity of Cu(II) adsorption onto CBC sorbent. As shown in Fig. S8 and Table S4 (Supporting information), the negative ΔG^0 values across all examined temperatures confirmed the favorable and spontaneous nature of Cu(II) adsorption. Furthermore, the increasing ΔG^0 with rising temperature suggested that elevated temperatures enhance adsorption spontaneity, which is consistent with the observed improvements in adsorption efficiency under higher thermal conditions. The positive ΔH^0 value of 45.74 kJ/mol indicated the endothermic nature of Cu(II) adsorption, aligning with previous reports by Salem *et al.* [35]. Additionally, the positive ΔS^0 value of 239.25 J mol^{-1} K^{-1} indicates a higher level of disorder at the solid-liquid interface during adsorption, likely due to structural rearrangements in both adsorbate and adsorbent phases that created a more disordered interfacial system [18].

The regeneration of CBC sorbent was evaluated using several eluents, including EDTA-2Na, CH_3COOH, CH_3COONa, HCl, and NaOH. As depicted in Fig. 2a, EDTA-2Na outperformed other eluents, achieving a remarkable re-adsorption capacity of 240.69 mg/g for Cu(II). This represents a 329.42 % improvement over 1.0 mol/L HCl regeneration treatment (56.05 mg/g). To ensure adsorption saturation during the re-adsorption assay, the initial Cu(II) concentration was slightly above the theoretical capacity. Notably, sodium carbonate formed during citrate-modified biomass pyrolysis may serve as an adsorption site for Cu(II). However, acidic eluents could potentially damage these sites, thereby impairing sorbent regeneration. In contrast, EDTA-2Na acts as an effective chelating agent by forming soluble complexes with surface-adsorbed Cu(II) [36], facilitating HMs removal and preserving the sorbent's structural integrity for subsequent reutilization. Reusability tests revealed that the sorbent regenerated with EDTA-2Na retained a Cu(II) capacity of 182.88 mg/g after four cycles (Fig. 2b), which is 26.85 % lower than the maximum capacity observed during the first cycle (240.69 mg/g). Despite this decrease, the retained capacity surpasses most reported biochar sorbents, highlighting CBC's potential for practical applications [31,37,38].

CBC sorbent's Cu(II) adsorption performance was further evaluated in high-salinity environments, including Na_2SO_4, NaCl solutions, and a real waste salt brine. Fig. 3a shows that the adsorption capacities were maintained around 227.33 ± 4.15 mg/g across Na_2SO_4 concentrations (0.1–0.5 mol/L). Notably, even when the salt strength was abruptly increased to a near-saturated level (1.4 mol/L, 20 °C), the adsorption capacity remained robust at 232.55 ± 6.36 mg/g. Concurrently, NaCl concentration effects were investigated (Fig. 3b), revealing that Cu(II) adsorption capacities in NaCl solutions (254.98 ± 13.18 mg/g) remained comparable to those in the salt-free condition (255.99 ± 16.07 mg/g). Similarly, the adsorption performance remained substantial at 252.14 ± 1.09 mg/g even at abruptly elevated NaCl concentrations (4.1 mol/L). These observations align with Chen *et al.* [18], who proposed that background electrolytes neutralize biochar surface positive charges, enabling Cl^- to bind to the biochar sorbent and effectively attract Cu(II). In contrast to Wang *et al.* [17], who observed reduced

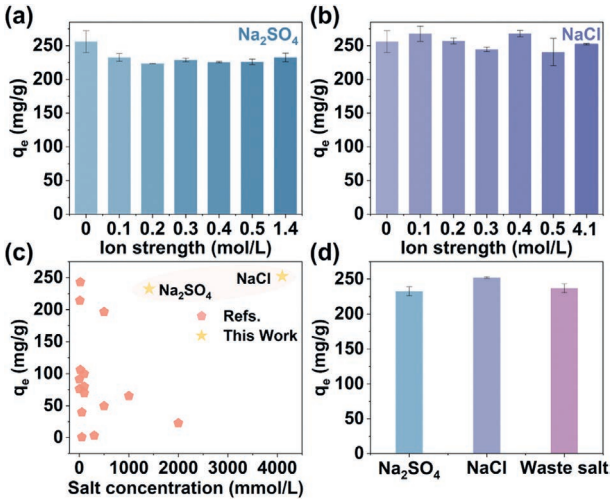


Fig. 3. The effect of (a) Na_2SO_4 and (b) NaCl salt strength on Cu(II) adsorption capacity. (c) A comparative analysis of Cu(II) adsorption performances under various saline conditions as reported in the literature, and (d) the Cu(II) adsorption capacity of CBC sorbent in a real waste salt brine, compared with the synthetic Na_2SO_4 and NaCl solutions.

heavy metal adsorption on microplastics (polystyrene/polyethylene terephthalate) with increasing salinity due to competitive Na^+ cation exchange, the CBC sorbent exhibited little effect on Cu(II) adsorption under elevated NaCl concentrations. This divergence suggests that electrostatic attraction may not be the dominant mechanism for Cu(II) adsorption. Fig. 3c and Table S5 (Supporting information) compared CBC and other reported sorbents, demonstrating CBC's superior salt tolerance and efficient Cu(II) adsorption. Furthermore, the test using a real waste salt brine achieved a Cu(II) adsorption capacity of 236.89 ± 6.36 mg/g, validating its practical applicability (Fig. 3d). Consequently, these results highlight the CBC sorbent's ability to maintain consistently high adsorption performance across various high-salinity conditions, effectively addressing challenges associated with recycling real high-salinity wastewater.

X-ray diffraction (XRD) analysis was performed to characterize CBC materials before and after Cu(II) adsorption. Fig. 4a shows sodium carbonate (Na_2CO_3, PDF #08–0448 and PDF #19–1130) as the primary crystalline phase, which formed through thermal decomposition of sodium citrate during pyrolysis (Eq. 1), consistent with Liu *et al.* [16]. Additionally, calcium carbonate ($CaCO_3$, PDF #47–1743) was also detected, possibly originating from the inherent calcium content of raw camphor bark biomass.

$$2Na_3C_6H_5O_7 \rightarrow 3Na_2CO_3 + 9C + 5H_2O \quad (1)$$

Post-adsorption XRD patterns under salt-free and salt-saturated conditions both revealed the presence of posnjakite ($Cu_4(SO_4)(OH)_6{\cdot}2H_2O$, PDF #43–0670), which is a basic copper sulphate mineral, implying that mineral precipitation mediated by the carbonates in biochar and sulfate in solution represents a primary mechanism for Cu(II) capture. This observation aligns with Liu *et al.* [16], who observed $Cu_2(OH)_3Cl$ formation in citrate-modified biochar. Previous studies indicated that the $Cu(OH)_2$ can be formed *via* carbonate replacement and hydrolysis [39], while Bakhtiari and Darezereshki [40] proposed that $Cu_4(SO_4)(OH)_6$ could form from the reaction between $CuSO_4$ and Na_2CO_3. Gao *et al.* [41] similarly identified posnjakite (001) peak at approximately 12.6° in Cu-BC350, further supporting the precipitation mechanisms involved with calcite and Cu^{2+} (such as $CuSO_4$) species. Additionally, the high-salinity environment does not influence the posnjakite formation. Instead, the elevated ionic strength may

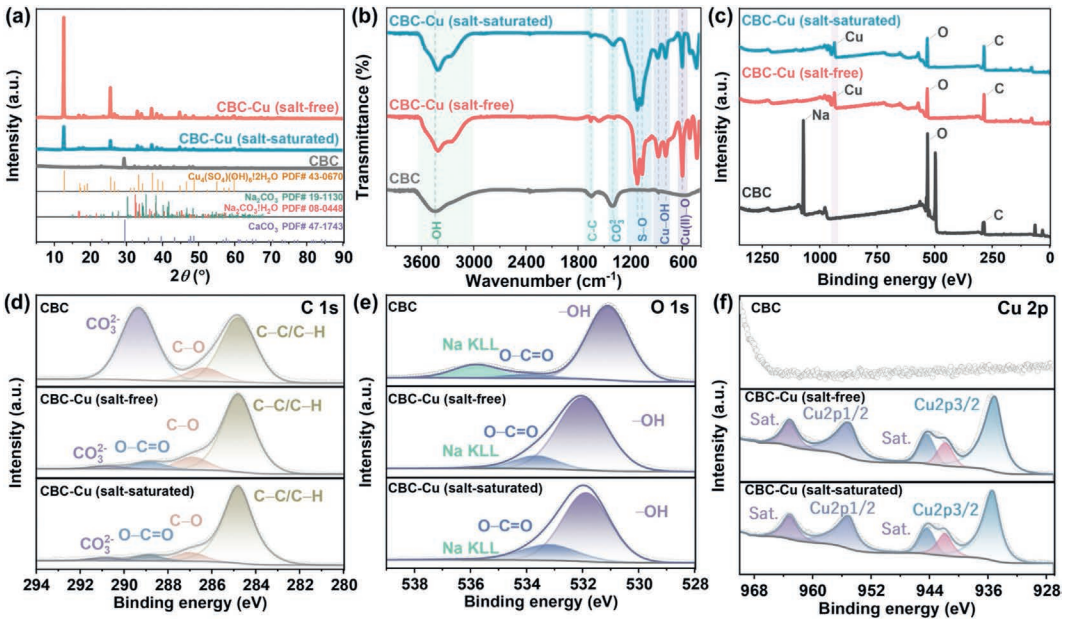


Fig. 4. The patterns of (a) XRD, (b) FTIR, (c) survey XPS and the high-resolution spectra for (d) C 1s, (e) O 1s, and (f) Cu 2p of the pristine CBC sorbent, as well as the Cu(II)-adsorbed CBC sorbent in salt-free and salt-saturated conditions.

enhance the mobility of ions in the solution, potentially accelerating reaction rates between Cu(II), sulfate, and carbonate species. The continuous supply of carbonate ions from the biochar-borne Na_2CO_3 and $CaCO_3$ ensures a steady-state availability of reactants for posnjakite formation, even in the presence of competing ions in the saline solution. This resilience of the precipitation mechanism under high-salinity conditions highlights the advantage of using CBC as a sorbent for Cu(II) removal from complex wastewater matrices.

Fourier-transform infrared (FTIR) analysis characterized the changes in surface chemistry of CBC before and after Cu(II) adsorption (Fig. 4b). The pristine CBC displays distinctive spectral features compared to the Cu(II)-adsorbed CBC. Pristine CBC exhibits a 1380 cm^{-1} peak from CO_3^{2-} asymmetric stretching [42], while Cu-adsorbed samples show a new peak at 1065 cm^{-1} corresponding to asymmetric stretching vibrations of the S – O bond in the SO_4^{2-} group [42,43]. This result also confirmed the posnjakite ($Cu_4(SO_4)(OH)_6{\cdot}2H_2O$) formation, which is consistent with XRD. Additionally, notable spectral variations between the pristine and Cu(II)-adsorbed CBC were observed in the 550–1000 cm^{-1} range. Peaks at 873 and 790 cm^{-1} are assigned to the bending vibrations of the Cu–OH group with differing hydrogen bond configurations [43], while a peak at 597 cm^{-1} corresponds to Cu(II)–O [40,44], indicating that Cu(II) coordinates with oxygen-containing functional groups on the surface of the CBC may also contribute to the Cu(II) adsorption process. A broad peak observed at around 3433 cm^{-1}, assigned to –OH group, displays a blue shift after adsorbing Cu(II) [37,45], implying the possible formation of inner-sphere surface complexes [45]. However, an additional peak at around 3253 cm^{-1} was observed, which differs from previous reports. This peak is attributed to H-bonding within the product, possibly originating from the structural hydroxyl groups in $Cu_4(SO_4)(OH)_6$ [46]. Therefore, the presence of this peak highlights the structural integration of water molecules into the precipitated phase. This aligns with the findings of Bakhtiari and Darezereshki [40], who characterized $Cu_4(SO_4)(OH)_6$ and identified vibration frequencies at 426, 487, 511, 601, 735, 780, 875, 943, 988, 1088, 1126, 1431, 3275, and 3391 cm^{-1}. Besides, the range of 480–585 cm^{-1} may correspond to Cu(II)–O. Therefore, these collective findings strongly confirm posnjakite ($Cu_4(SO_4)(OH)_6{\cdot}2H_2O$) as the dominant copper-containing phase. Additionally, the peak near 1650 cm^{-1}, associated with C=C stretching vibrations [18,47], narrowed significantly after Cu(II) adsorption. This emphasizes the biochar's aromatic structure and implies the occurrence of π-π interactions [47,48], along with potential π-electron coordination with heavy metal ions [49].

The X-ray photoelectron spectroscopy (XPS) analysis was further conducted to gain insights into the underlying mechanisms of Cu(II) adsorption onto CBC, and the parameters are summarized in Table S7 (Supporting information). The survey spectra confirmed the presence of new copper peaks in both salt-free and salt-saturated samples, confirming Cu(II) adsorption successfully (Fig. 4c). High-resolution C 1s spectra of pristine CBC were deconvoluted into C–C/C–H (284.8 eV), C–O (285.53 eV), O–C=O (287.15 eV), and CO_3^{2-} (289.61 eV) (Fig. 4d). Notably, the peak at 289.61 eV was absent in the adsorbed samples, indicating that carbonates played a role in the adsorption process, likely *via* hydrolysis. This hydrolysis released OH^-, elevating local pH and promoting $Cu(OH)_2$ formation, which then reacted with SO_4^{2-} to form posnjakite, as confirmed by XRD. Meanwhile, O 1s XPS spectra of pristine CBC showed a peak at 536.08 eV attributed to Na KLL Auger electrons, confirming the formation of sodium carbonate *via* pyrolysis of citrate-impregnated biomass at 650 °C [50]. Post-adsorption spectra revealed significant decreases in CO_3^{2-} and Na^+ atomic percentages, further indicating the involvement of Na_2CO_3 in Cu(II) removal. Different from previous studies that reported CO_3^{2-} can form complexes and/or coprecipitate with Cu(II) to generate $CuCO_3$ [28], this study did not detect $CuCO_3$ through XRD analysis. Instead, the slight shifts in C–O and O–C=O peaks after adsorption suggest that Cu(II) coordinated with oxygen lone pairs, lowering electron density around the C atom and increasing C binding energy [51].

O 1s XPS spectra of pristine CBC were deconvoluted into three distinct peaks located at 531.36 eV (–OH), 534.19 eV (O–C=O), and 536.08 eV (Na KLL) (Fig. 4e), confirming Na_2CO_3 formation *via* citrate pyrolysis [50]. Post-adsorption spectra showed significant decreases in Na KLL intensity, further indicating the involvement of Na_2CO_3 in Cu(II) removal. This observation aligns with the find-

ings from Gao *et al.* [41] and Wei *et al.* [52], who observed efficient Cu(II) adsorption by biochar, resulting in posnjakite formation and a notable decrease in C–O groups in C 1s spectra of Cu-BC350/550. Similarly, Yan *et al.* [45] observed a C–O content reduction from 32.02 % to 21.87 % after Cu(II) adsorption, alongside increased C=O content, suggesting surface complexation between Cu(II) and oxygen-containing functional groups may contribute to adsorption. The –OH peak shifted 0.52–0.64 eV to a higher binding energy, indicating the presence of primary adsorption sites arising from the hydrolysis of Na_2CO_3. Besides, the peak at 531.36 eV may also overlap with contributions from SO_4^{2-} and/or OH^- derived from $Cu_4(SO_4)(OH)_6{\cdot}2H_2O$ [53]. The relative content (%) of the peak at 534.19 eV increased after Cu(II) adsorption under both salt-free and salt-saturated conditions, likely reflecting bound water in the posnjakite structure [54,55]. As shown in Fig. 4f, the peaks for Cu $2p_{3/2}$ and Cu $2p_{1/2}$ were observed at binding energies of 935.32 and 954.96 eV ($\Delta_{metal} = 19.64$ eV) in the salt-free condition, and at 935.38 and 955.06 eV ($\Delta_{metal} = 19.68$ eV) in the salt-saturated condition, respectively. Satellite peaks at 943.68 Hongand 963.12 eV (7–10 eV from the main peaks) confirmed the successful adsorption of Cu(II) ions by the CBC sorbent [56], with the end product being $Cu_4(SO_4)(OH)_6{\cdot}2H_2O$.

During adsorption, the hydroxyl group may serve as the primary adsorption site for Cu(II), while oxygen-containing functional groups are likely engaged in surface complexation. In a previous study, the displacement of carbonate ions by $Cu(OH)_2$ intermediates may also lead to the formation of basic copper carbonate precipitates, which maintained stability across salinity conditions [39]. Similarly, the underlying adsorption mechanisms (Fig. S15 in Supporting information) in this work involve sodium carbonate formation during citrate pyrolysis. This mineral phase undergoes hydrolysis, releasing hydroxide ions within biochar micropores and creating an alkaline microenvironment that facilitates the formation of $Cu(OH)_2$ intermediates. In the salt-containing solution, these intermediates further react with SO_4^{2-} to form posnjakite ($Cu_4(SO_4)(OH)_6{\cdot}2H_2O$), reinforcing the role of coupled hydrolysis and precipitation mechanisms in immobilizing Cu(II) ions on the CBC surface. These mechanisms further contribute to the negligible decline in Cu(II) adsorption capacity under salt-containing conditions by enabling continuous generation of hydroxide ions *via* carbonate hydrolysis, thereby ensuring efficient Cu(II) removal and robust anti-salt interferences. Additionally, surface complexation with oxygen-containing groups provides supplementary adsorption, though non-dominant. Although the complexation between copper and oxygen-containing groups on the biochar persisted in saline conditions, this process was slightly affected by the salt and remains non-dominant in Cu(II) adsorption.

This work fabricated a sorbent for Cu(II) adsorption with excellent ability for anti-salt interference and a remarkable adsorption capacity of 251.21 mg/g. The sorbent exhibited recyclability, achieving four adsorption cycles. Moreover, it displayed superior Cu(II) removal performance in a real waste salt brine, attaining a q_e of 236.89 mg/g. Adsorption behavior may be dominated by physical and monolayer adsorption on a homogeneous surface, with spontaneous and endothermic characteristics. Oxygen-containing groups, particularly hydroxyl group (–OH), were pivotal in Cu(II) adsorption. The primary mechanisms involved surface precipitation and complexation, contributing to the formation of posnjakite ($Cu_4(SO_4)(OH)_6{\cdot}2H_2O$).

Declaration of competing interest

The authors declare that they have no known competing financial interests or personal relationships that could have appeared to influence the work reported in this paper.

CRediT authorship contribution statement

Xianxin Luo: Writing – original draft, Methodology, Investigation, Formal analysis, Data curation, Conceptualization. **Jianhao Xu:** Methodology, Investigation, Data curation, Conceptualization. **Qi Luo:** Methodology, Investigation. **Yan Xiao:** Methodology, Investigation. **Feng Wei:** Methodology, Conceptualization. **Meitong Li:** Methodology, Conceptualization. **Wenjiao Yuan:** Methodology, Conceptualization. **Penghui Shao:** Writing – review & editing, Supervision, Conceptualization. **Shenglian Luo:** Writing – review & editing, Supervision, Conceptualization.

Acknowledgments

This study was financially supported by the Key Research and Development Program of Jiangxi Province (No. 20232BBG70008), the National Key Research and Development Program of China (No. 2023YFC3905903), and the National Natural Science Foundation of China (No. 52470149).

Supplementary materials

Supplementary material associated with this article can be found, in the online version, at doi:10.1016/j.cclet.2025.111914.

References

[1] M. Bilal, J.A. Shah, T. Ashfaq, et al., J. Hazard. Mater. 263 (2013) 322–333.
[2] P. Shao, Z. Chang, M. Li, et al., Nat. Commun. 14 (2023) 1365.
[3] C.C. Nie, X.G. Li, S.X. Shi, et al., Sep. Purif. Technol. 322 (2023) 124277.
[4] B.K. Biswal, B. Zhang, P. Thi Minh Tran, et al., Chem. Soc. Rev. 53 (2024) 5552–5592.
[5] T.K. Sankar, P.Meshram Abhilash, Rev. Environ. Contam. Toxicol. 262 (2023) 5.
[6] H.A. Shamkhi, A.D.Z. Albdiri, F.A. Jabir, D. Petruzzelli, Arab. J. Sci. Eng. 47 (2022) 5705–5719.
[7] Z. Zhao, W. Xu, Z. Wang, et al., PLoS One 16 (2021) e0256101.
[8] Z. Zhao, W. Qin, J. Long, et al., Environ. Sci. Pollut. Res. 30 (2023) 21671–21682.
[9] Q. Chen, D. Zhou, Y. Zhu, et al., Desalination 590 (2024) 117985.
[10] N. Wang, H. Quan, B. Tan, et al., Desalination 592 (2024) 118086.
[11] Z. Liang, W. Yang, Z. Yin, et al., Desalination 587 (2024) 117921.
[12] A.M. Elgarahy, K.Z. Elwakeel, S.H. Mohammad, G.A. Elshoubaky, J. Environ. Chem. Eng. 8 (2020) 103915.
[13] M. Radenković, J. Petrović, S. Pap, et al., Chemosphere 347 (2024) 140684.
[14] T. Zhao, Y. Yao, D. Li, et al., Sci. Total Environ. 640-641 (2018) 73–79.
[15] B.K. Biswal, R. Balasubramanian, J. Environ. Chem. Eng. 11 (2023) 110986.
[16] Y. Liu, L. Zhang, Z. Zhang, et al., J. Environ. Manage. 301 (2022) 113819.
[17] X. Wang, R. Zhang, Z. Li, B. Yan, Sci. Total Environ. 812 (2022) 152573.
[18] L. Chen, J. Hu, Y. He, et al., Sep. Purif. Technol. 342 (2024) 127070.
[19] T. Li, W. Zhang, S. Zhai, et al., Water Res. 143 (2018) 87–98.
[20] Y. Chen, Y. Liu, Y. Li, et al., Water Air Soil Pollut. 231 (2020) 404.
[21] A. Bogusz, P. Oleszczuk, R. Dobrowolski, Bioresour. Technol. 196 (2015) 540–549.
[22] T.M.A. Babeker, S. Lv, M.N. Khalil, et al., Sep. Purif. Technol. 354 (2025) 129436.
[23] F.P. Dad, W.U.D. Khan, F. Sharif, A.S. Nizami, Environ. Res. 241 (2024) 117702.
[24] A. Kumar Mondal, C. Hinkley, S. Kondaveeti, et al., Bioresour. Technol. 414 (2024) 131562.
[25] K. Vikrant, K.H. Kim, E.E. Kwon, D.W. Boukhvalov, Chem. Eng. J. 433 (2022) 133497.
[26] Z. Huang, B. Chang, Y. Tang, et al., J. Water Process Eng. 67 (2024) 106209.
[27] X. Ma, Y. Cao, J. Deng, et al., Chem. Eng. J. 492 (2024) 152189.
[28] C. Jiang, F. Yue, C. Li, et al., J. Environ. Chem. Eng. 10 (2022) 108996.
[29] O.C.S. Al Hamouz, S.A. Ali, Sep. Purif. Technol. 98 (2012) 94–101.
[30] S. Senniappan, S. Palanisamy, V.Manon Mani, et al., Environ. Res. 235 (2023) 116676.
[31] J. Zhang, X. Xia, K. Li, et al., Chem. Eng. J. 479 (2024) 147657.
[32] S. Pap, Q. Zhao, I. Cakin, et al., Chem. Eng. J. 494 (2024) 152848.
[33] C. Liu, X. Yan, H.-X. Zhang, et al., Heliyon 10 (2024) e35169.
[34] B. Choudhary, D. Paul, J. Environ. Chem. Eng. 6 (2018) 2335–2343.
[35] D.B. Salem, A. Ouakouak, F. Touahra, et al., Bioresour. Technol. 383 (2023) 129225.
[36] X. Huang, J. Yang, J. Wang, et al., Chemosphere 206 (2018) 513–521.
[37] H. Chen, Y. Pan, W. Zhang, et al., Chem. Eng. J. 495 (2024) 153356.
[38] Z. Zhou, B. Zhao, Y. Zhang, et al., Desalin. Water Treat. 166 (2019) 24–34.
[39] J. Liu, W. Cheng, X. Yang, Y. Bao, Sci. Total Environ. 704 (2020) 135252.
[40] F. Bakhtiari, E. Darezereshki, Mater. Lett. 65 (2011) 171–174.
[41] X. Gao, H. Zhang, J. Zhang, et al., Bioresour. Technol. 394 (2024) 130259.
[42] Z. Jin, Y.F. Xiao, M.D. Xu, et al., J. Iran. Chem. Soc. 21 (2024) 2295–2304.

[43] E.K. Güner, D. Kancan, J. Naktiyok, A. Özer, Asia-Pac. J. Chem. Eng. 16 (2021) e2583.
[44] M. Guedes, J.M.F. Ferreira, A.C. Ferro, J. Colloid Interface Sci. 330 (2009) 119–124.
[45] J. Yan, X. Zuo, S. Yang, et al., J. Hazard. Mater. 424 (2022) 127435.
[46] E.A. Secco, Can. J. Chem. 66 (1988) 329–336.
[47] T.J. Jiang, H.M. Morgan, W.T. Tsai, et al., Sustainability 16 (2024) 6623.
[48] Z. Li, M. Li, Z. Wang, X. Liu, Chem. Eng. J. 381 (2020) 122785.
[49] J. Ma, W. Huang, X. Zhang, et al., J. Environ. Chem. Eng. 9 (2021) 104703.
[50] D.T. Hopkins, S. MacQuarrie, K.A. Hawboldt, J. Environ. Manage. 303 (2022) 114270.
[51] Y. Bai, D. Lei, L. Li, et al., J. Environ. Chem. Eng. 12 (2024) 114630.
[52] Y. Wei, T. Chen, Z. Qiu, et al., Bioresour. Technol. 365 (2022) 128146.
[53] M.C. Biesinger, Surf. Interface Anal. 49 (2017) 1325–1334.
[54] C. Zhang, Y. Cao, M. Zhang, et al., Chem. Eng. Sci. 286 (2024) 119665.
[55] Y. Wang, Y. Chen, C. Liu, et al., Chem. Eng. J. 316 (2017) 936–950.
[56] T. Wen, Y. Zhao, X. Jiao, et al., J. Clean. Prod. 293 (2021) 126184.